$$Cr(O^tBu)_4 + LiPPh_2 \xrightarrow{THF} LiCr(O^tBu)_4 + \tfrac{1}{2}Ph_2PPPh_2 \quad (3)$$

by ^{31}P NMR spectroscopy) is the only phosphorus-containing product. $LiCr(O^tBu)_4$, also insoluble (cf. $KCr(O^tBu)_4$), was identified by its conversion to $Cr(O^tBu)_4$ upon reaction with CuCl.

We feel that the weight of evidence indicates that only *inner-sphere* electron transfer is effective at interconverting $Cr(O^tBu)_4^-$ and $Cr(O^tBu)_4$. Thus, eq 3 would proceed through a $(^tBuO)_{4-n}Cr(O^tBu)_nLiPPh_2$ bridged species. The reaction of $Cr(O^tBu)_4^-$ with CuCl could then proceed by an analogous bridged intermediate. In fact, when CuCl is added to a blue slurry of $KCr(O^tBu)_4$ in THF, the color changes to dark brown before the blue color of $Cr(O^tBu)_4$ develops. Attempts to stabilize this brown preredox intermediate in THF by carrying out this reaction in the presence of 3 equiv of PPh_3/equiv of CuCl gave a light purple solution, which decomposed to $Cr(O^tBu)_4$ and Cu^0 over a 24-h period. When the complex formed in THF from CuCl and 2 equiv of PMe_2Ph was added to $KCr(O^tBu)_4$, the solution became deep purple (more stable than with PPh_3) but decomposed to green upon attempted crystallization.

It was observed that $KCr(O^tBu)_4$ reacts with $^1/_2$ equiv of $[Rh(COD)Cl]_2$ in either Et_2O or THF to give an intermediate yellow-green solution. The benzene-soluble component of this product ($(COD)RhCr(O^tBu)_4$?) subsequently decays to $Cr(O^tBu)_4$. Attempts to improve on this approach to an isolable inner-sphere electron-transfer intermediate are currently under way.

We have tested the hypothesis that electron transfer must occur by an inner-sphere mechanism by attempting the reduction of $Cr^{IV}(O^tBu)_4$ by the 19-valence-electron species Cp_2Co. Even at reflux temperature (9 h) in benzene there is no reaction, as indicated by persistence of the ^1H NMR signals of both reagents (Cp_2Co at −51 ppm in C_6D_6). Also unreactive are the outer-sphere reductants $Cr(CO)_6$ and $W(CO)_6$ (reflux in THF).

To summarize, the steric crowding observed in the structure of $Cr(O^tBu)_4$ accounts both for its lack of polymerization (compare smaller alkoxides) and lack of adduct formation with Lewis bases. Its observed reaction chemistry is dominated by electron transfer, but the steric shielding does not preclude alkoxide bridging to Lewis acidic redox reagents and, thus, apparent inner-sphere redox mechanisms. The ease of oxidation of $Cr(O^tBu)_4^-$ (assuming tetrahedral geometry for the CrO_4 unit) to the unusual oxidation state Cr(IV) probably originates in the relatively high energy of the t_2 HOMO in the anion.

Acknowledgment is made to the donors of the Petroleum Research Fund, administered by the American Chemical Society, to the Norwegian Research Council for Science and the Humanities, and to VISTA for support of this research.

Contribution from the Department of Chemistry, Faculty of Science, Fukuoka University, Nanakuma, Jonan-ku, Fukuoka 814-01, Japan, and Department of Electronic Chemistry, Tokyo Institute of Technology, Nagatsuta, Midori-ku, Yokohama 227, Japan

X-ray Diffraction Study of Calcium(II) Chloride Hydrate Melts: $CaCl_2 \cdot R H_2O$ (R = 4.0, 5.6, 6.0, 8.6)

Toshio Yamaguchi,*,† Shun-ichi Hayashi,‡ and Hitoshi Ohtaki‡,§

Received November 2, 1988

X-ray scattering measurements have been performed on calcium(II) chloride hydrate solutions, $CaCl_2 \cdot RH_2O$, with R = 4.0 (120 °C), 5.6 (72 °C), 6.0 (33 °C), and 8.6 (25 °C). The analysis of the radial distribution functions and model fittings revealed that in the solution of $CaCl_2 \cdot 8.6H_2O$ a Ca^{2+} ion is surrounded by six water molecules, the Ca^{2+}–OH_2 distance being 245 pm. With decreasing H_2O concentration a direct Ca^{2+}–Cl^- correlation owing to the formation of contact ion pairs appears at 270 pm. About one Cl^- ion binds to a Ca^{2+} ion in the $CaCl_2 \cdot 6H_2O$ melt, whereas about two Cl^- ions coordinate to a Ca^{2+} ion in the $CaCl_2 \cdot 4.0H_2O$ melt, whose structure is similar to that found in the crystal structure of $CaCl_2 \cdot 4H_2O$. The structure of the $CaCl_2 \cdot 6H_2O$ melt, which always yields supercooling, was investigated at 15 °C below the melting point (29.9 °C) and 80 °C. The structure in the supercooled state is similar to that found at 33 °C but different from that of $CaCl_2 \cdot 6H_2O$ crystal. A tendency of further Cl^- ion coordination to the Ca^{2+} ion with increasing temperature was observed.

Introduction

Electrolyte solutions may be classified into five categories depending on the water content according to Braunstein:[1] (I) very dilute aqueous solution, (II) concentrated aqueous solution, (III) hydrate melts, (IV) melts containing incomplete hydration sheaths, and (V) anhydrous molten salts. Most of structural studies so far reported have been devoted to categories I, II, and V. On the contrary, there appeared very few structural investigations on III and IV, in which ion–ion interactions become comparable with ion–water interactions. These solutions, which are called "hydrate melts", are of considerable interest from a structural point of view whether or not a structure change occurs through a melting/crystallization process between the solid and liquid phases. Hydrate melts are also paid attention as heat storage materials[2] in industrial applications, among which calcium(II) chloride hexahydrate[2c-f] is one of the most attractive materials from the standpoint of the melting temperature, heat storage density, and thermal stability.

The structure of concentrated aqueous $CaCl_2$ solutions classified into category II has been investigated by NMR[3] and Raman[4] spectra, self-diffusions,[5] X-ray[6] and neutron[7] diffraction, and

* To whom correspondence should be addressed.
† Fukuoka University.
‡ Tokyo Institute of Technology.
§ Present address: Coordination Chemistry Laboratories, Institute for Molecular Science, Myodaiji-cho, Okazaki 444, Japan.

(1) Braunstein, J. *Ionic Interaction (I)*; Academic Press: New York, 1971.
(2) (a) Marcus, Y. In *Molten Salt Technology*; Lovering, D. G., Ed.; Plenum: New York, 1982. (b) Gawron, K.; Schröder, J. *Energy Res.* **1977**, *1*, 351. (c) Carlsson, B.; Stymne, H.; Wettermark, G. *Sol. Energy* **1979**, *23*, 343. (d) Carlsson, B.; Wettermark, G. *Sol. Energy* **1980**, *24*, 239. (e) Bajnóczy, G.; Zöld, A. *Appl. Energy* **1982**, *10*, 97. (f) Kimura, H.; Kai, J. *Sol. Energy* **1984**, *33*, 49.
(3) Vogrin, B. F. J.; Knapp, P. S.; Flint, W. L.; Anton, A.; Highberger, G.; Malinowski, E. R. *J. Chem. Phys.* **1971**, *54*, 178.
(4) Kanno, H.; Hiraishi, J. *J. Phys. Chem.* **1983**, *87*, 3664.
(5) (a) Lyons, P. A.; Riley, J. F. *J. Am. Chem. Soc.* **1954**, *76*, 5216. (b) Hertz, H. G.; Mills, R. *J. Phys. Chem.* **1978**, *82*, 952.
(6) (a) Albright, J. N. *J. Chem. Phys.* **1972**, *56*, 3783. (b) Licheri, G.; Piccaluga, G.; Pinna, G. *J. Chem. Phys.* **1976**, *64*, 2437. (c) Licheri, G.; Piccaluga, G.; Pinna, G. *J. Am. Chem. Soc.* **1979**, *101*, 5438. (d) Caminiti, R.; Licheri, G.; Paschina, G.; Piccaluga, G.; Pinna, G. *Z. Naturforsch.* **1980**, *35A*, 1361.

0020-1669/89/1328-2434$01.50/0

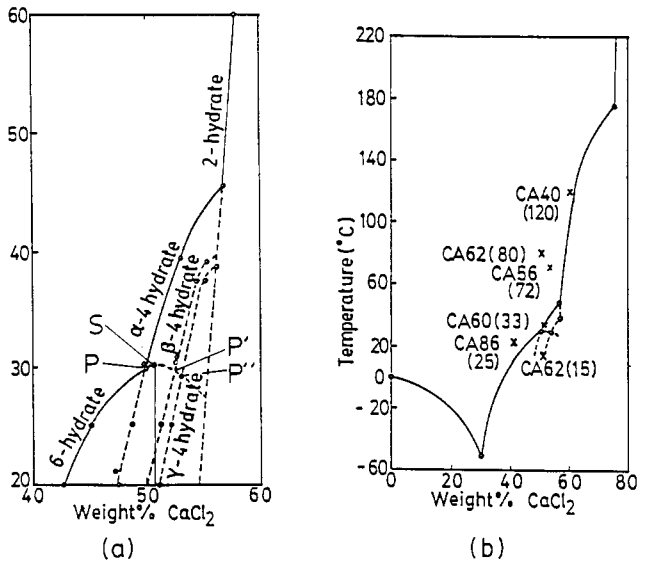

Figure 1. (a) Phase diagram of the $CaCl_2$–H_2O system. (b) Compositions of sample solutions investigated (×). The numbers in parentheses show the temperatures employed. Further information on sample composition is given in Table I.

molecular dynamics simulation.[8] According to the phase diagram for the $CaCl_2$–H_2O system,[2c-f] there exist mono-, di-, tetra-, and hexahydrates in the solid state (see Figure 1a). In addition, the tetrahydrate forms metastable β- and γ-phases together with the thermodynamically stable α-phase. In the vicinity of the hexahydrate there are three peritectica (P, P', and P'') and the melting point maximum (S). Thus, during the cooling of a solution with the composition of the hexahydrate, the α-tetrahydrate starts to precipitate at 32 °C, the β-phase at 22 °C, and the γ-phase at 18 °C.[2c] Since calcium(II) chloride hexahydrate yields supercooling down to 10–14 °C (mp 29.9 °C), structural analysis of the liquid phase of the hexahydrate at various temperatures is an interesting subject to understand a crystallization phenomenon. Recently, Licheri et al.[6c,d] performed an X-ray scattering measurement of $CaCl_2 \cdot 6H_2O$ melt near room temperature and reported that the short-range ordering is similar to that found in the hexahydrate crystal.

In the present study, we measured X-ray scatterings from $CaCl_2 \cdot RH_2O$ solutions with R = 4.0, 5.6, 6.0, and 8.6; the structure at each composition was determined and compared with those of crystalline $CaCl_2 \cdot 4H_2O$ and $CaCl_2 \cdot 6H_2O$ hydrates, the corresponding solid phase. The structure of molten $CaCl_2$[9] was also determined as an anhydrous case of the above melts. In the case of the $CaCl_2 \cdot 6H_2O$ solution, X-ray scatterings were also measured in the supercooled state (15 °C), above the melting point (33 °C), and at 80 °C to examine structural similarities between the solutions at each temperature and the crystals of the α-, β-, and γ-tetrahydrates and the hexahydrate.

Experimental Section

Sample Preparation and Analysis. Commercially available $CaCl_2 \cdot 2H_2O$ of reagent grade was recrystallized from water and dried in vacuo. The composition of the crystals obtained was determined from the stoichiometry on the basis of the chloride content determined by gravimetry with an aqueous silver nitrate solution. Sample solutions of the composition $CaCl_2 \cdot RH_2O$ with R = 4.0, 5.6, 6.0, 6.2, and 8.6 were prepared by mixing a required amount of distilled water with the crystals. The Ca^{2+} concentration was determined by EDTA titration. The densities of the sample solutions below 100 °C were determined at the temperatures of X-ray measurements by using pycnometers, whereas that of $CaCl_2 \cdot 4H_2O$ at 120 °C was determined by use of naphthalene as a reference solvent with an electric furnace. The compositions of the sample solutions thus obtained are summarized in Table I and in Figure 1b. The data for molten $CaCl_2$ were quoted from the work by Iwamoto et al.[9]

Table I. Composition of $CaCl_2 \cdot RH_2O$ Solutions Investigated (mol dm^{-3})[a]

	$[Ca^{2+}]$	$[Cl^-]$	$[H_2O]$	R	d/g cm^{-3}	t/°C
CA00[b]	18.7	37.3	0	0	2.07	800
CA40	8.41	16.8	33.6	4.0	1.54	120
CA56	7.45	14.9	41.4	5.6	1.57	72
CA60	6.92	13.8	41.5	6.0	1.51	33
CA62	6.84	13.7	42.1	6.2	1.52	15
CA62	6.66	13.3	40.9	6.2	1.48	80
CA86	5.33	11.0	45.8	8.6	1.42	25

[a] d and t are the density and the temperature of X-ray measurements, respectively. [b] Reference 9.

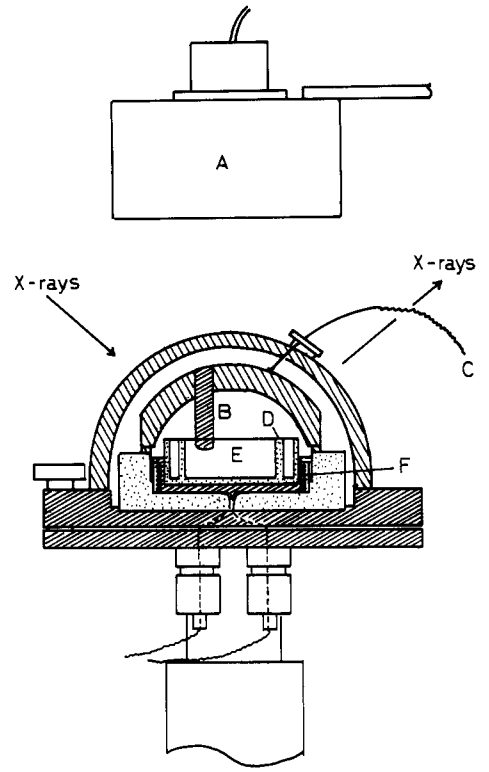

Figure 2. Schematic view of a furnace used for high-temperature X-ray scattering measurements: (A) infrared lamp; (B) thermocouple; (C) thermister; (D) cell; (E) sample solution; (F) heater.

X-ray Scattering Measurements. X-Ray scattering measurements were made on the reflection geometry by using a JEOL θ–θ diffractometer. Mo Kα (λ = 71.07 pm) was used as an X-ray source, and the scattered X-rays from the free surface of a sample solution were monochromatized by Johansson type LiF(200) and graphite(002) crystals for solutions CA86 and CA60 and for the other solutions, respectively. The scattered X-ray intensities were measured as the time used to collect 40 000 counts at each discrete angle (2θ) from 2 to 140° (2θ is the scattering angle), corresponding to the scattering vector s ($=4\pi(\sin\theta)/\lambda$) from 3.1×10^{-4} to 0.167 pm^{-1}. The measurements were scanned two or three times, depending on the counting statistics, and the data sets obtained agreed with each other within 2%. The measurements at temperatures above 25 °C were made by use of a furnace shown in Figure 2. Details of the measurements and the diffractometer have been described elsewhere.[10]

Data Analysis. The measured intensities were corrected for background, absorption, polarization, and incoherent scatterings and scaled to the electron units by comparing the asymptote of the experimental data

(7) (a) Cummings, S.; Enderby, J. E.; Howe, R. A. *J. Phys. C* **1980**, *13*, 1. (b) Hewish, N. A.; Neilson, G. W.; Enderby, J. E. *Nature* **1982**, *297*, 138.

(8) (a) Probst, M. M.; Bopp, P.; Heinzinger, K.; Rode, B. M. *Chem. Phys. Lett.* **1984**, *106*, 317. (b) Probst, M. M.; Radnai, T.; Heinzinger, K.; Bopp, P.; Rode, B. M. *J. Phys. Chem.* **1985**, *89*, 753. (c) Pálinkás, G.; Heinzinger, K. *Chem. Phys. Lett.* **1986**, *126*, 251.

(9) Iwamoto, N.; Umesaki, N.; Asahina, T.; Kosaka, M. *Nippon Kagaku Kaishi* **1982**, *6*, 920.

(10) (a) Ohtaki, H.; Maeda, M.; Itoh, S. *Bull. Chem. Soc. Jpn.* **1974**, *47*, 2217. (b) Ohtaki, H.; Yamaguchi, T.; Maeda, M. *Bull. Chem. Soc. Jpn.* **1976**, *49*, 701. (c) Yamaguchi, T.; Johansson, G.; Holmberg, B.; Maeda, M.; Ohtaki, H. *Acta Chem. Scand.* **1985**, *A38*, 437.

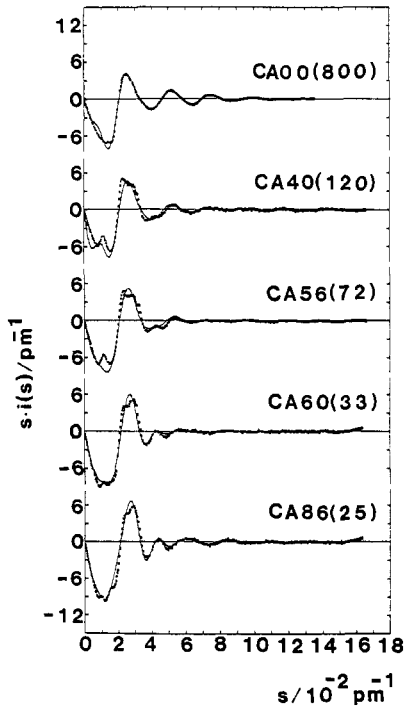

Figure 3. *s*-weighted structure functions of hydrate melts CA86 (25 °C), CA60 (33 °C), CA56 (72 °C), CA40 (120 °C), and CA00 (800 °C): (dots) experimental values; (solid lines) values calculated by using the model parameters given in Table II.

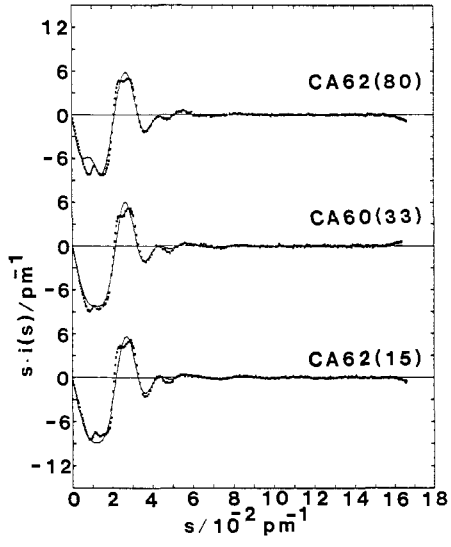

Figure 4. *s*-weighted structure functions of hydrate melts CA62 (15 °C), CA60 (33 °C), and CA62 (80 °C): (dots) experimental values; (solid lines) values calculated by using the model parameters given in Table II.

with the calculated coherent intensities at large scattering angles ($\theta > 50°$). The scaling factor thus calculated agreed within 2% with that obtained by the integration method. Details of the data treatments were reported previously.[10,11]

The structure function $i(s)$ is obtained by subtracting the independent scatterings from all atoms in the sample solutions from the scaled intensities $I(s)$:

$$i(s) = I(s) - \sum x_i f_i(s)^2 \qquad (1)$$

where x_i is the number of the ith atom in the stoichiometric volume V containing one Ca atom and $f_i(s)$ is the coherent scattering factor corrected for the real and imaginary parts of the anomalous dispersion. The coherent and incoherent scattering factors of neutral atoms were taken from ref 12. The structure functions multiplied by the scattering vector

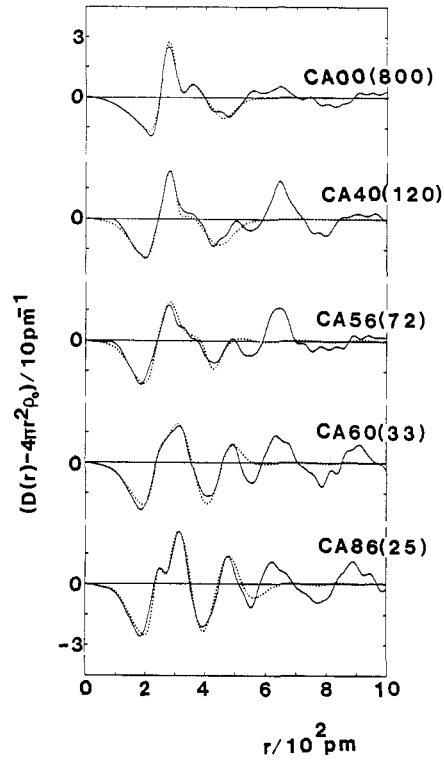

Figure 5. Radial distribution functions in the form $D(r) - 4\pi r^2\rho_0$ for hydrate melts CA86 (25 °C), CA60 (33 °C), CA56 (72 °C), CA40 (120 °C), and CA00 (800 °C): (solid lines) experimental values; (dots) values calculated by using the model parameters given in Table II.

s are shown in Figure 3 for solutions CA86 (25 °C), CA60 (33 °C), CA56 (72 °C), CA40 (120 °C), and CA00 (800 °C) and in Figure 4 for CA62 (15 and 80 °C) and again for CA60 (33 °C) for comparison.

The radial distribution function is calculated by the Fourier transform of the structure function:

$$D(r) = 4\pi r^2\rho_0 + \frac{2r}{\pi}\int_0^{s_{max}} s\, i(s)\, M(s) \sin(sr)\, ds \qquad (2)$$

where ρ_0 is the average electron density in the stoichiometric volume V, and s_{max} is the maximum s value available in the measurements. A modification function $M(s)$ of the form $[\sum x_i f_i^2(0)/\sum x_i f_i^2(s)]\exp(-100s^2)$ was used in all cases.

The theoretical structure function calculated on the basis of a model is obtained by

$$i(s)_{calcd} = \sum\sum x_i n_{ij} f_i f_j \frac{\sin(sr_{ij})}{sr_{ij}} \exp(-b_{ij}s^2) - \sum\sum x_i x_j f_i f_j \frac{4\pi R_j^3}{V} \frac{\sin(sR_j) - sR_j\cos(sR_j)}{(sR_j)^3} \exp(-B_j s^2) \qquad (3)$$

The first term of eq 3 is related to the short-range interactions characterized by the interatomic distance r_{ij}, the temperature factor b_{ij}, and the number of interactions n_{ij} for atom pairs ij. The second term arises from the interaction between a spherical hole and the continuum electron distribution beyond the above discrete distance. R_j is the radius of the spherical hole around the jth atom and B_j the softness parameter for emergence of the continuum electron distribution. All the calculations were carried out by use of a program KURVLR.[11]

Results and Discussion

Radial Distribution Functions. Figure 5 shows the radial distribution functions in the form $D(r) - 4\pi r^2\rho_0$ obtained for solutions CA86 (25 °C), CA60 (33 °C), CA56 (73 °C), and CA40 (120 °C). The function of molten salt CA00 (800 °C)[9] is also included for comparison. Peaks are observed at 245, 320, and 470 pm for CA86. The peak at 245 pm is ascribed to the Ca^{2+}–H_2O interactions within hydrated Ca^{2+} ions on the basis of the crystal structure of $CaCl_2 \cdot 6H_2O$[13] and the sum of the ionic radius[14] of

(11) Johansson, G.; Sandström, M. *Chem. Scr.* **1973**, *4*, 195.
(12) *International Tables for X-ray Crystallography*; Kynoch Press: Birmingham, England, 1964; Vol. 4.
(13) Leclaire, P. A.; Borel, M.-M. *Acta Crystallogr.* **1977**, *B33*, 2938.
(14) Shannon, R. D. *Acta Crystallogr.* **1976**, *A32*, 751.

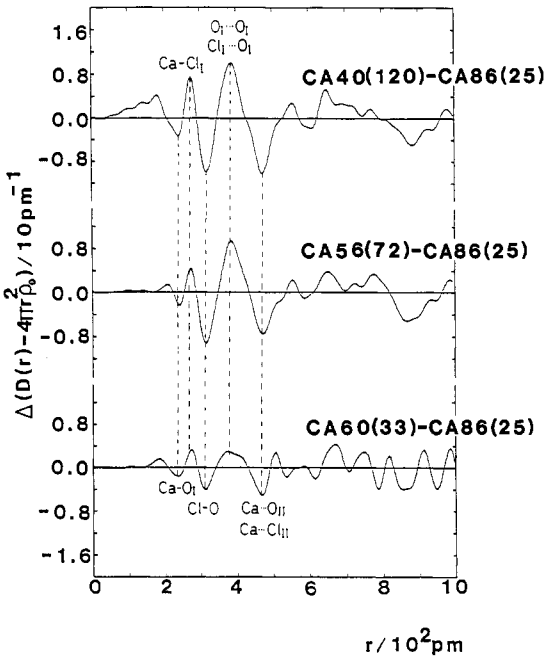

Figure 6. Difference radial distribution functions $\Delta(D(r) - 4\pi r^2\rho_0)$ between hydrate melts CA60 (33 °C), CA56 (72 °C), or CA40 (120 °C) and CA86 (25 °C).

Ca^{2+} and the size of a water molecule (~140 pm). The second peak at 320 pm arises mainly from the Cl^-–H_2O interactions due to the anion hydration[6,8] and in part from the interactions between the water molecules in the first and second coordination shells, which often appear around 290 pm in aqueous solutions.[6] To the peak centered at 470 pm may contribute several long-range interactions such as the interactions between a central Ca^{2+} ion and Cl^- or H_2O present in the second coordination shell.[8] With decreasing concentration of water, the features of the radial distribution functions change gradually, indicating that structure change occurs in these solutions.

In order to make the change in the peaks clearer, the difference radial distribution functions were obtained by subtracting the radial distribution function for CA86 from those for the other solutions. As clearly seen in Figure 6, with the decrease in water content, the Ca^{2+}–OH_2 interactions at 245 pm decreased, whereas a new peak developed at 280 pm. The new peak can be attributed to Ca^{2+}–Cl^- interactions due to the penetration of Cl^- ion into the first coordination shell of Ca^{2+}, since the value of 280 pm is very close to the Ca–Cl interatomic distance found in the crystal structures of $CaCl_2 \cdot 2H_2O$[15] and $CaCl_2 \cdot 4H_2O$[16] and moreover the sum of the ionic radii[14] of Ca^{2+} and Cl^-. On the other hand, the peak at 320 pm, which is given as a valley in the figure and ascribed to the Cl^-–H_2O interactions due to the Cl^- hydration, decreased with increasing solute concentration. In addition, the peak at 360 pm, which arises from the interligand interactions such as H_2O···H_2O and Cl^-···H_2O pairs, increased, but the peak at 470 pm from the second-neighbor Ca^{2+}···H_2O and Ca^{2+}···Cl^- interactions decreased; thus, the minimum in the figure became deeper in the case of the CA40–CA85 curve than in the CA60–CA85 curve.

Model Fittings. On the basis of the above considerations about the radial distribution functions, we performed a quantitative analysis to determine the structural parameters by means of a least-squares method, in which a function U was minimized

$$U = \sum_{s_{min}}^{s_{max}} s^4[i_{obsd}(s) - i_{calcd}(s)]^2 \qquad (4)$$

where s_{max} and s_{min} are the maximum and minimum of the s value used in the calculations.

A structure model employed for the solutions is as follows.

(a) The first coordination shell of Ca^{2+} ion consists of both H_2O (later abbreviated as O_I) and Cl^- (abbreviated as Cl_I) and is characterized in terms of their interatomic distances r_{ij}, temperature factors b_{ij}, and number of interactions n_{ij}, which were allowed to vary. The interligand interactions such as O_I–O_I and Cl_I–O_I pairs were also included with their independent parameters (r, b, n).

(b) The interactions between the water molecules (O_I) or Cl^- ions (Cl_I) bound to a Ca^{2+} ion and the water molecules (O_{II}) in the second coordination shell were taken into account; their distances, temperature factors, and the number of interactions were allowed to vary independently.

(c) The interactions between the Ca^{2+} ion and the water molecules (O_{II}) or Cl^- ions (Cl_{II}) in the second coordination shell were included by use of their interatomic distances, temperature factors, and the number of interactions.

(d) Hydration of Cl^- ions was represented as the first-neighbor Cl^-–H_2O interactions with their distance, temperature factor, and coordination number.

(e) The interatomic Ca^{2+}···Ca^{2+} interactions were considered on the basis of the crystal structures of the tetra- and hexahydrates of $CaCl_2$.[13,16] In the case of molten $CaCl_2$ the Cl^-···Cl^- interactions were also taken into consideration, which should occur in the anhydrous salt.[9]

(f) The interactions appearing at distances longer than those described above were approximated in terms of the continuous distribution of electrons.

The least-squares calculations were performed over the whole s range for all solutions by the use of program NLPLSQ.[17] The results finally obtained are summarized in Table II. [Errors in r and n are estimated as ±2 pm and ±0.3, respectively, for the first neighbor Ca–O_I and Ca–Cl_I interactions, but for the interactions in the medium-range order, the errors became larger than these because of significant correlations among the parameters allowed to vary.]

$CaCl_2 \cdot 8.6H_2O$ (25 °C). According to the result of the least-squares calculation, a Ca^{2+} ion is surrounded by about six water molecules, presumably in an octahedral form. The number of water molecules around the Cl^- ion is about 6. Both results are very similar to previous findings from X-ray scattering studies of concentrated (~3 M) aqueous $CaCl_2$ solutions.[6] In the second coordination sphere about six Cl^- ions were found to exist; thus, the water molecules in the first hydration sphere of Ca^{2+} are probably shared with both Ca^{2+} and Cl^- ions in the solution CA86 at 25 °C.

$CaCl_2 \cdot 6.0H_2O$ (33 °C). As seen in Table II, about one Cl^- ion penetrates into the first coordination shell of Ca^{2+} ion in this solution. Accordingly, the number of interligand Cl^-···O_I interactions increases, whereas that of the O_I···O_I interactions decreases. The second-neighbor Ca^{2+}···O_{II} and Ca^{2+}···Cl_{II} interactions also decrease. The present findings for CA60 differ from a previous result by Licheri et al.[6c,d] derived from an X-ray scattering measurement of a solution of the composition $CaCl_2 \cdot 6H_2O$. They observed three peaks at ~240, 275, and 320 pm in their $G(r)$ ($=D(r)/4\pi r^2\rho_0$), which are not resolved in the present distribution function (Figure 5). Although $G(r)$ sharpens the variation in the radial distribution function as r becomes smaller, this difference in the distribution function should rather be ascribed to different solute concentration of sample solutions used in the two experiments. In ref 6d they described the molarity of the "$CaCl_2 \cdot 6H_2O$" sample to be 6.3 mol dm^{-3}, which corresponds to a $CaCl_2$ solution less concentrated than the $CaCl_2 \cdot 6H_2O$ solution. It should be noted that the composition of the present sample solution, rigorously adjusted at $CaCl_2 \cdot 6.0H_2O$, is 6.92 mol dm^{-3} (see Table I). Thus, for the present CA60 an increase in the interaction at 275 pm, expected from the difference distribution functions in Figure 6, will result in the unresolved peaks around 275 pm. In their model

(15) Leclaire, P. A.; Borel, M. M. *Acta Crystallogr.* **1977**, *B33*, 1608.
(16) (a) Leclaire, P. A.; Borel, M. M. *Acta Crystallogr.* **1979**, *B35*, 585. (b) Leclaire, P. A.; Borel, M. M. *Acta Crystallogr.* **1978**, *B34*, 900. (c) Leclaire, P. A.; Borel, M. M.; Monier, J. C. *Acta Crystallogr.* **1980**, *B36*, 2757.

(17) Yamaguchi, T. Doctoral Thesis, Tokyo Institute of Technology, 1978.

Table II. Structural Parameters Used in the Model Calculations for $CaCl_2 \cdot RH_2O$ Solutions[a]

		CA86 (25 °C)	CA62 (15 °C)	CA60 (33 °C)	CA62 (80 °C)	CA56 (72 °C)	CA40 (120 °C)	CA00 (800 °C)
$Ca-O_I$	r/pm	244	244	245	245	244	246	
	n	6.0	5.9	5.6	5.3	4.8	3.9	
$Ca-Cl_I$	r/pm		275	274	274	275	280	276
	n		0.9	1.0	1.4	1.7	2.1	5.4
O_I-O_{II}	r/pm	292	291	294	294	295	293	
	n	1.9	2.2	1.7	2.0	1.9	0.9	
Cl-O	r/pm	326	321	321	321	323	324	
	n	5.8	4.9	4.5	4.5	3.9	4.4	
O_I-O_I	r/pm	350	347	347	347	356	378	
	n	11.7	8.4	8.3	9.5	5.4	3.7	
Cl_I-O_I	r/pm		363	363	364	367	382	
	n		4.4	4.2	4.8	5.7	7.7	
Ca-Ca	r/pm	405	410	402	405	396	426	341
	n	0.5	0.6	0.5	1.4	2.8	2.2	4.2
Cl-Cl	r/pm							386
	n							7.8
$Ca-O_{II}$	r/pm	460	450	460	460	448	454	
	n	5.9	5.0	5.0	3.8	2.8	1.0	
$Ca-Cl_{II}$	r/pm	470	475	480	480	480		
	n	5.9	5.2	5.0	4.5	3.2		
Ca	R/pm	498	476	473	470	463	446	398
Cl	R/pm	499	496	495	480	467	465	446
O	R/pm	305	334	303	303	303	292	

[a] r and n are the interatomic distance and the number of interactions, respectively.

fits two peaks at 240 and 275 pm were interpreted in terms of three short and six long Ca–O interactions, respectively, on the basis of the crystal structure of the $CaCl_2 \cdot 6H_2O$ hydrate. Our difference distribution functions with increasing solute concentration, however, show a gradual increase in the peak at 275 pm, which arises from the $Ca-Cl_I$ interactions. Thus, we believe that the interaction at 275 pm should be ascribed to a $Ca-Cl_I$ contact formed by Cl^- ion penetration into the first coordination shell of Ca^{2+} ion and that the crystal structure model proposed by them is not a unique one to reproduce the experimental data. Concerning the medium-range order in CA60, the analysis of the radial distribution functions and least-squares fits (Table II) suggested that calcium and chloride ions occupy the positions similar to those in $CaCl_6 \cdot 6H_2O$. This result is consistent with previous findings.[6c,d]

$CaCl_2 \cdot 5.6H_2O$ (72 °C) and $CaCl_2 \cdot 4.0H_2O$ (120 °C). According to the results shown in Table II, more Cl^- ions penetrate into the first coordination shell of Ca^{2+} ion; on an average about 1.7 and 2.1 Cl^- ions are bound to a Ca^{2+} ion in CA56 and CA40, respectively. Since the sum of $n(Ca-O_I)$ and $n(Ca-Cl_I)$ is about 6, the coordination number for Ca^{2+} is retained at about 6 even when water molecules are replaced by Cl^- ions in the first coordination shell. A similar coordination number was also obtained for molten $CaCl_2$ (see Table II).

Comparison with Crystal Structures. The crystal structures of $CaCl_2 \cdot 6H_2O$[13] and the α-,[16a] β-,[16b] and γ-phases[16c] of $CaCl_2 \cdot 4H_2O$ have been reported. The structure of α-$CaCl_2 \cdot 4H_2O$ consists of $[CaCl_2 \cdot 4H_2O]_2$ units held together by hydrogen bonds; the coordination number of a Ca^{2+} ion is 7, with two Cl atoms at 285 pm, one Cl atom at 293 pm, and four H_2O molecules at 235–246 pm. In β-$CaCl_2 \cdot 4H_2O$ a calcium atom is surrounded by two Cl atoms at 274 pm and four water molecules at 233 pm, the octahedral unit being connected by hydrogen bonds. γ-$CaCl_2 \cdot H_2O$ consists of two types of Ca coordination; one type of a calcium ion is surrounded by six Cl atoms (273–275 pm), and the other, by one Cl atom (287 pm) and seven water molecules (243–285 pm). In the crystal structure of $CaCl_2 \cdot 6H_2O$,[13] on the other hand, a calcium atom is surrounded by nine water molecules (three at 245 pm and six at 259 pm), which are hydrogen-bonded with Cl atoms sitting in the outer sphere.

We compared the above crystal structures with the most likely models of the hydrate melts with similar compositions in Table II. The structure model of CA40 obtained in the present study is similar to that found for the β-$CaCl_2 \cdot 4H_2O$. The structure of hydrate melt CA60 contains an octahedral moiety consisting of one Cl atom and five water molecules around a Ca^{2+} ion. The

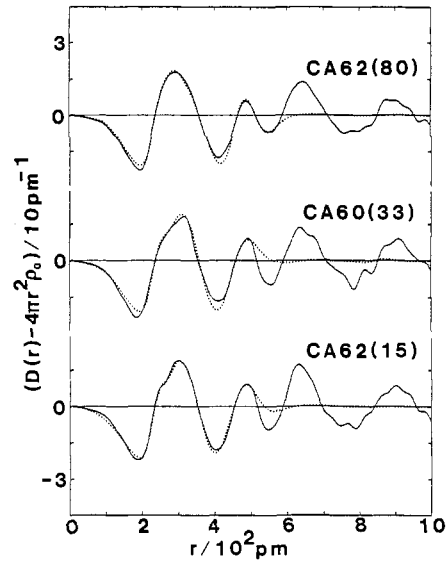

Figure 7. Radial distribution functions in the form of $D(r) - 4\pi r^2\rho_0$ between hydrate melts CA62 (15 °C), CA60 (33 °C), and CA62 (80 °C): (solid lines) experimental values; (dots) values calculated by using the model parameters given in Table II.

present finding thus indicates that the structure change occurs through the melting process of $CaCl_2 \cdot 6H_2O$. This structural difference between the solution and crystal would be responsible for supercooling. The surroundings of Ca^{2+} and Cl^- ions in the $CaCl_2 \cdot 6H_2O$ crystal are rather similar to those found for CA86.

Temperature Effect on the Structure of $CaCl_2 \cdot 6H_2O$. Figure 7 shows the radial distribution functions of solution CA62 at 15 °C (the supercooled state) and 80 °C, together with that of CA60 at 33 °C. Apparently, the shape of the first peak centered at 300 pm changes with temperature, but those of the peaks at the longer distance do not differ appreciably, indicating that no drastic change in the long-range order of the solution occurs at the three temperatures. The changes in the peaks are more clearly observed in the difference radial distribution functions (Figure 8) obtained by taking a difference between the radial distribution functions at the three temperatures. In the difference function between CA62(80) and CA62(15) a $Ca-O_I$ peak at 245 pm appears in the negative direction, a $Ca-Cl_I$ peak at 275 pm appears in the positive one, the interligand $O_I \cdots O_I$ and $Cl_I \cdots O_I$ peaks appear in

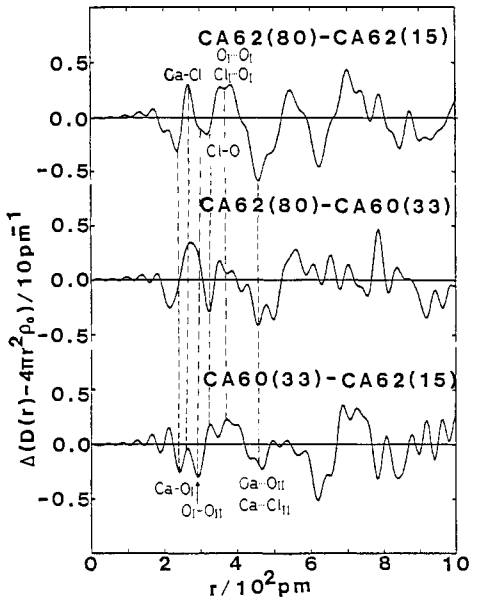

Figure 8. Difference radial distribution functions in the form of $\Delta(D(r) - 4\pi r^2\rho_0)$ between two of hydrate melts CA62 (15 °C), CA60 (33 °C), and CA62 (80 °C).

the positive one, and the second neighbor $Ca\cdots O_{II}$ and $Ca\cdots Cl_{II}$ peaks at 470 pm appear in the negative one. These trends are also found in the difference function between CA62(80) and CA60(33). These changes in the peaks are similar to those observed in Figure 6, in which we compared the solutions with different concentrations, and the results are interpreted in terms of exchange of bound water molecules with Cl^- ions in the first coordination sphere of Ca^{2+} ion.

On the basis of the above considerations, the model fitting was performed for the structure functions of CA62 at 15 and 80 °C. Models were employed along the same guideline mentioned in the previous section. The final results thus obtained are given in Table II. An increase in temperature resulted in a decrease in the $Ca-O_I$ interactions, an increase in the $Ca-Cl_I$ ones, and a decrease in the second-neighbor $Ca\cdots O_{II}$ and $Ca\cdots Cl_{II}$ interactions; the results indicate that water molecules bound to a Ca^{2+} ion are gradually exchanged with Cl^- ions to form contact Ca^{2+}–Cl^- ion pairs. On the other hand, the structure parameter (n) obtained for CA62(15) suggests that aquated Ca^{2+} ions are more stable in the supercooled state. From a comparison between the structures of CA62(15) and solids $CaCl_2\cdot 4H_2O$ and $CaCl_2\cdot 6H_2O$ we can conclude that there is no structural similarity between the supercooled solution and the tetra- and hexahydrates of $CaCl_2$. This structural difference will cause the supercooling of the hexahydrate. The position of the solution CA62 at 80 °C is near that of CA56 at 72 °C in the phase diagram (see Figure 1b); correspondingly, both structures are similar, as seen from the results in Table II.

Acknowledgment. This work has been financially supported, in part, by the Ministry of Education, Science, and Culture of Japan (Grant-in-Aid for Scientific Research on Priority Area of Macromolecular Complexes No. 63612005). All the calculations were performed at the Computer Centers of Tokyo Institute of Technology and Fukuoka University.

Registry No. $CaCl_2$, 10043-52-4; H_2O, 7732-18-5; Ca, 7440-70-2.

Contribution from the NRC "Demokritos", GR-153 10 Aghia Paraskevi Attikis, Greece, Physics Department, Ioannina University, GR-451 10 Ioannina, Greece, and Kifissias Av. 108, GR-115 26 Athens, Greece

Pillaring of Montmorillonite by Organotin Cationic Complexes

D. Petridis,*,† T. Bakas,‡ A. Simopoulos,† and N. H. J. Gangas§

Received November 8, 1988

The intercalation of dimethyltin(IV) cationic clusters in montmorillonite leads to an organotin–clay complex exhibiting a basal spacing of 1.66 ± 0.02 nm. The maximum cluster loading is larger than expected on the basis of the cation-exchange capacity of the clay and the formal charge of monomeric tin complexes, indicating intercalation of organotin oligomers. The thermal transformation of the intercalated montmorillonite to pillared clay was studied via XRD, ^{119}Sn Mössbauer, and IR spectroscopies. Calcination above 250 °C leads to a collapsed interlayer space. However, calcination after glycerol solvation of the precursor at 240 °C leads to a tin oxide pillared clay that is stable up to about 500 °C. This result is attributed to a lower interlayer acidity upon displacing interlayer water with glycerol. The above treatment of the precursor opens a new route to the synthesis of pillared clays.

I. Introduction

During the last decade a novel class of microporous materials has emerged from the intercalation of swelling clays, i.e. smectites, with oligo- or polymeric cationic complexes of metals.[1] By calcination of the intercalates, the complexes inserted in the clay interlayer space transform into metal oxide pillars, which support the silicate sheets and keep them apart even at elevated temperatures (up to about 600 °C). Thus, the structure of pillared layered clays (PILC's) consists of a labyrinth of pores with sizes in the 1–10-nm range with a total surface area between 200 and 500 m^2/g, while a pronounced Brønsted and Lewis acidity prevails in the interlayer space. Therefore, PILC's offer a novel host material for molecular sorption, chemical synthesis, and catalysis under conditions of high selectivity, imposed by steric and electronic constraints of this super-zeolitic structure. The early recognition that PILC's have important potential applications (e.g. in petroleum cracking[2]) has stimulated research on the synthesis of new PILC's, on the understanding of the transformations occurring upon firing the PILC precursor, and on the elucidation of the role that the pillars play in the physicochemical processes in the interlayer space.

The list of metal oxides used in pillaring various smectites is rapidly expanding and comprises already quite a few metals, e.g. aluminum, zirconium, silicon, chromium, iron, titanium, niobium,

† NRC "Demokritos".
‡ Ioannina University.
§ Kifissias Av. 108.

(1) (a) Brindley, G. W.; Sempels, R. E. *Clay Miner.* **1977**, *12*, 229. (b) Pinnavaia, T. J. *Science* **1983**, *220*, 365. (c) Fripiat, J. J. *Clays Clay Miner.* **1986**, *34*, 501.
(2) (a) Vaughan, D. E. W.; Lussier, R. J. In *Proceedings of the 5th International Conference on Zeolites*; Rees, L. V., Ed.; Heyden: London, 1980; p 94. (b) Occelli, M. L. *Ind. Eng. Chem. Prod. Res. Dev.* **1983**, *22*, 553.

0020-1669/89/1328-2439$01.50/0